Received: 25 November 2016 | Revised: 30 December 2016 | Accepted: 9 January 2017

DOI 10.1002/aoc.3750

FULL PAPER

WILEY Applied Organometallic Chemistry

Three novel Ni(II), VO(II) and Cr(III) mononuclear complexes encompassing potentially tridentate imine ligand: Synthesis, structural characterization, DNA interaction, antimicrobial evaluation and anticancer activity

Laila H. Abdel-Rahman[1] | **Ahmed M. Abu-Dief**[1] | **Maram Basha**[2] | **Azza A. Hassan Abdel-Mawgoud**[1]

[1] Chemistry Department, Faculty of Science, Sohag University, 82524 Sohag, Egypt

[2] Department of Chemistry, Faculty of Science, Alfaisaliah Campus, King Abdulaziz University, Jeddah, Saudi Arabia

Correspondence
Ahmed M. Abu-Dief, Chemistry Department, Faculty of Science, Sohag University, 82524 Sohag, Egypt.
Email: ahmed_benzoic@yahoo.com

Three novel Cr(III),VO(II) and Ni(II) imine complexes derived from the condensation of 2-aminophenol (AP) with 2-hydroxynaphthaldehyde (HN) were synthesized. The prepared HNAP imine ligand and its complexes were investigated via various physicochemical tools. The results suggest that the parent ligand behaves as a dibasic tridentate ONO ligand, when coordinated to Cr(III) in octahedral and to Ni(II) in tetrahedral geometry. In the case of VO(II), it coordinates in distorted square pyramidal geometry. Also, the prepared compounds were screened for their antimicrobial activities against pathogenic bacteria, *Escherichia coli* (−ve), *Bacillus subtilis* (+ve) and *Staphylococcus aureus* (+ve), and some types of fungi, *Aspergillus niger*, *Candida glabrata* and *Trichophyton rubrum*. The results indicate that the complexes show a stronger antimicrobial efficiency compared to the pro-ligand. The interaction of the prepared complexes with calf thymus DNA was investigated using spectral, viscosity and gel electrophoresis measurements. The obtained results clearly demonstrate that the binding affinity with calf thymus DNA follows the order HNAPCr > HNAPV > HNAPNi. The cytotoxic activity of the prepared compounds on human colon carcinoma cells (HCT-116 cell line), hepatic cellular carcinoma cells (HepG-2cell line) and breast carcinoma cells (MCF-7cell line) was examined. From these results it is found that the investigated complexes have potent cytotoxicity against growth of carcinoma cells compared to the corresponding imine pro-ligand.

KEYWORDS
anticancer activity, antimicrobial activity, DNA interaction, imine ligand, thermal analyses, Vo(ii)

1 | INTRODUCTION

Imine ligands are considered privileged ligands, because they are easily prepared by a simple one-pot condensation of aldehydes and primary amines in an alcohol solvent. Their ease of synthesis, multi-denticity (from monodentate to hexadentate), combination of donor atoms (complexion usually through the imine nitrogen and other atoms like oxygen, sulfur or nitrogen) and stability have made them the preferred ligand systems in catalysis, biological modelling, design of molecular ferromagnets, liquid crystals,[1–3] medical imaging[4] and optical materials.[5] Moreover, imine ligands are able to coordinate many different metals,[6–9] and to stabilize them in various oxidation states. Furthermore, imine complexes have been used as drugs and they have a wide variety of antimicrobial activities against bacteria and fungi, and activity

against certain types of tumours.[10–12] Some drugs have increased activity when administered as metal chelates and inhibit the growth of tumours.[12,13]

The interest in vanadium coordination chemistry is promoted by the presence of this element in biological systems,[14,15] and by the catalytic[16] and medicinal[17] properties of its compounds. The potential catalytic abilities of vanadium compounds have led to a great interest in vanadium coordination chemistry in recent years.[9] Thus, in the present paper, we report the synthesis of a tridentate imine ligand of 2-aminophenol (AP) and 2-hydroxynaphthaldehyde (HN). The structure of the prepared HNAP imine ligand was checked using ^{1}H NMR, ^{13}C NMR, infrared (IR) and UV–visible spectroscopies. Then its Cr(III), VO(II) and Ni(II) complexes were prepared and the spectral and thermal properties of these complexes were studied in detail. Also the kinetic parameters for the degradation steps in thermograms of these complexes were calculated. The biological activity of the pro-ligand and its complexes was determined against selected kinds of bacteria and fungi. Moreover, the interaction of the complexes with calf thymus DNA (CT-DNA) was studied. Furthermore, the anticancer activity of the prepared imine complexes was investigated.

2 | EXPERIMENTAL

2.1 | Reagents

All of the solvents and chemicals used for our study were of commercially available reagent grade and used without purification. HN, AP, vanadyl acetylacetonate ($VO(C_5H_7O_2)_2$), chromium nitrate ($Cr(NO_3)_3{\cdot}6H_2O$) and nickel nitrate ($Ni(NO_3)_2{\cdot}6H_2O$) were obtained from Sigma-Aldrich. All reagents and solvents were commercially acquired from Merck, Aldrich or Fluka. CT-DNA, tris(hydroxymethyl) aminomethane (Tris), bromophenol blue dye and ethidium bromide were obtained from Sigma-Aldrich Chemie (Germany).

2.2 | Preparation of HNAP imine pro-ligand

An amount of 5 mmol (0.861 g) of HN was dissolved in ethanol and mixed with an ethanolic solution of 5 mmol (0.545 g) of AP. Then the mixture was refluxed and stirred for 2 h at 85 °C and s yellow precipitate was formed. The completion of the reaction mixture was monitored by TLC. The product was gathered by filtration, washed with ethanol and dried over anhydrous $CaCl_2$ (Scheme 1).

^{1}H NMR (DMSO, δ, ppm): 15.65 (s, OH), 10.15 (s, OH), 8.36–6.83 (m, 9H, aromatic), 9.49 (s, 1H, CH═N), 8.36 (s, 1H, $CH_{position10}$) (Figure S1). ^{13}C NMR (DMSO, δ, ppm): 177.17 (N═CH), 150.46, 149.11, 138.11, 134.36, 129.64, 129.41, 128.50, 127.19, 126.46, 125.21, 123.48, 120.31, 120.15, 118.31, 116.60, 108.35 for carbons of aromatic rings (Figure S2).

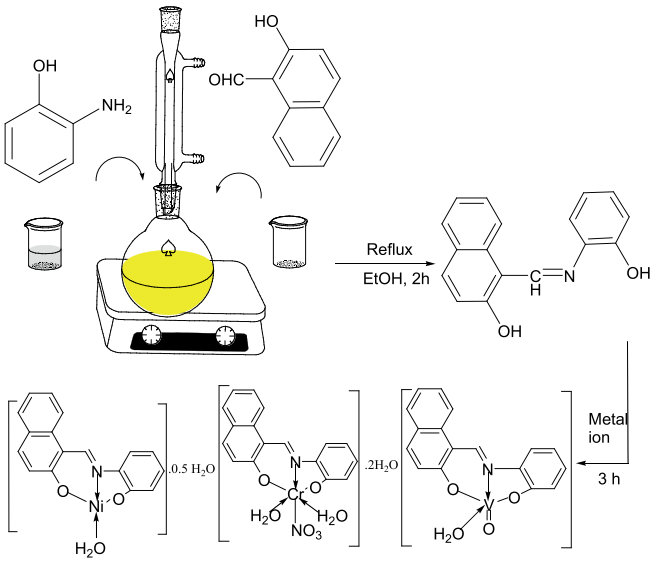

SCHEME 1 Synthetic strategy for preparation of investigated complexes and suggested structures

2.3 | Preparation of HNAPCr, HNAPNi and HNAPV imine complexes

Cr(III), VO(II) and Ni(II) imine complexes were obtained according to a general procedure: 10 mmol (2.63 g) of HNAP pro-ligand was dissolved in ethanol and 10 mmol of metal salt (4.00 g of Cr(III), 2.98 g of Ni(II) or 2.65 g of VO(II)) was dissolved in an aqueous ethanolic mixture. The two solutions were mixed together and refluxed for 2 h at 85 °C. After evaporation the solvent, the precipitated solid was filtered off from the reaction mixture, thoroughly washed with ethanol to remove any traces of unreacted starting materials, and dried under vacuum. The purity of the complexes was checked by TLC (Scheme 1).

2.4 | Characterization of prepared HNAP imine pro-ligand and its complexes

Melting point for the prepared imine ligand and decomposition temperatures of its complexes were measured with a melting point device (Gallenkamp, UK). IR spectra were recorded as KBr pellets using a Shimadzu FTIR-8300 spectrophotometer. ^{1}H NMR and ^{13}C NMR spectra were obtained in deuterated dimethylsulfoxide (DMSO) solutions with a Bruker Avance DPX-500 spectrometer. All of the scanning UV–visible spectra in DMF were recorded using 10 mm matched quartz cells with a PG spectrophotometer model T + 80. Elemental analyses were conducted at the main laboratory of Cairo University using an elemental analyser (PerkinElmer 240c). Magnetic susceptibility was

measured using a Gouy balance and diamagnetic corrections were executed by Pascal"s constants. Molar conductivity measurements were performed using a JENWAY 4510 conductivity meter. Thermogravimetric analysis was conducted under nitrogen with a heating rate 10 °C min^{-1} with a Shimadzu 60H analyser. The values of absorbance of 5×10^{-3} M of each complex were determined at various pH levels. The pH levels were checked using a series of Britton universal buffers.[11] An ADWA AD1000 and AD1020 pH meter at 298 K equipped with a CL-51B combined electrode was utilized for pH measurements, calibrated against standard buffers (pH 4.02 and 9.18) before measurements.

2.5 | Evaluation of stoichiometry of prepared imine complexes

The molar ratio[10–12,18] and continuous variation[10–12,19,20] methods were used. Metal salt and ligand solutions were mixed, stirred and allowed to equilibrate and the absorbance was read at λ_{max} up to 2 h. The sum of the metal ion concentration and HNAP imine pro-ligand concentration was 1×10^{-3} M for each solution. Ten volumetric flasks of 10.0 ml were used for the investigation. The initial concentrations of metal salt and HNAP pro-ligand were 1 mM. The absorbance of each solution was measured and plotted against the mole fraction of metal ion or mole fraction of the pro-ligand.

2.6 | Estimation of apparent formation constants of prepared complexes

The formation constants (K_f) of the studied imine complexes formed in solutions were obtained from spectrophotometric measurements using the continuous variation method.[10–12,18–20] according to the following relation:

$$K_f = \frac{A/A_m}{(1-A/A_m)^2 C} \quad (1)$$

where A_m is the absorbance at the maximum formation of the complex, A is arbitrarily selected absorbance values on either side of the absorbance peak and C is the initial molar concentration of the metal. Also, the free energy change, ΔG^*, of the complexes was determined using $\Delta G^* = -RT \ln K_f$, at 25 °C, where K_f is the formation constant, R is the gas constant and T is the temperature in kelvin.

2.7 | Kinetic studies

The kinetic parameters of the decomposition process for the metal complexes were determined using the Coats–Redfern integral method.[11,12,19,21] The energy of activation (E^*) for the decomposition of the metal complexes was determined employing the following equation:

$$\log\left[\frac{\log(w_\infty/(w_\infty - w))}{T^2}\right] = \log\left[\frac{AR}{\phi E^*}\left(1-\frac{2RT}{E^*}\right)\right] - \frac{E^*}{2.303RT} \quad (2)$$

where w_∞ is the mass loss at the completion of the decomposition reaction, w is the mass loss at temperature T, R is the universal gas constant and φ is the heating rate. Since $1 - 2RT/E^* \approx 1$, a plot of the left-hand side of equation (1) against $1/T$ gives a slope from which E^* was calculated and A was determined from the intercept. The other kinetic parameters, the entropy of activation (ΔS^*), enthalpy of activation (H^*) and activation free energy change (G^*), were calculated using the following expressions:[11,12,19,21]

$$\Delta S^* = 2.303R \log \frac{Ah}{K_B T} \quad (3)$$

$$\Delta H^* = E^* - RT \quad (4)$$

$$\Delta G^* = H^* - T\Delta S^* \quad (5)$$

where K_B and h are Boltzmann"s and Planck"s constants, respectively.

2.8 | Antibacterial and antifungal activities of prepared compounds

The *in vitro* biological activities of the HNAP imine pro-ligand and its complexes were examined against various types of bacteria (*Bacillus subtilis* (+ve), *Escherichia coli* (−ve) and *Staphylococcus aureus* (+ve)) by the well diffusion method using nutrient agar as the environment.[10–12,18–20] The antifungal activities of the compounds were also checked by the well diffusion method against various types of fungi (*Aspergillus niger*, *Candida glabrata* and *Trichophyton rubrum*) on potato dextrose agar as environment. The investigated compounds were dissolved in DMSO and solutions with concentrations of 10 and 20 mg ml^{-1} were prepared separately. In a typical method, a well was made on the agar medium vaccinated with microorganism.[11,12,18,22] Wells supplemented with DMSO and reference antibacterial drug served as negative and positive controls, respectively. The well filled with the test solution using a micropipette and the plate was incubated for 24 h at 37 °C for bacteria or 72 h at 35 °C for fungi. After incubation, the diameter of the obtained zone of inhibition around the sample was taken as a criterion of the inhibitory power of the sample against the particular test microbe as measured with a zone reader (Hi Antibiotic zone scale). The standard antibacterial drug gentamycin and antifungal drug fluconazol were also screened under similar conditions for comparison. In order to clarify the effect of

solvent (DMSO) on the biological screening, DMSO alone was used as control, and it showed no activity against microbial strains. The measurements were made in triplicate for each compound and their average values are reported.

2.9 | DNA binding study

2.9.1 | DNA binding propensity

All the tests including the interaction of the complexes with DNA were conducted in Tris–HCl buffer (60 mM, pH = 7.1). CT-DNA was purified by centrifugal dialysis before use. A solution of CT-DNA in the buffer gave a ratio of UV absorption at 260 and 280 nm of greater than about 1.85, suggesting that the DNA was sufficiently free from protein contamination.[11,12,18,22] The concentration of DNA per nucleotide was evaluated by monitoring the UV absorbance at 260 nm utilizing ε_{260} = 6600 mol^{-1} cm^2. The stock solution was stored at 4 °C and used within only one day.

2.9.2 | Electronic spectra for interaction of prepared complexes with DNA

All the tests including the interaction of the complexes with DNA were carried out in Tris–HCl buffer (60 mM, pH = 7.1). Spectrophotometric scan test was performed by keeping the complex concentration constant while changing the nucleic acid concentration in the surrounding conditions. The absorption due to free CT-DNA was removed by adding equimolar CT-DNA to clear buffer solution in the reference compartment and the spectra obtained were considered to result from the complexes and the DNA–metal complex aggregation.[12,18,22] From the absorption data, the intrinsic binding constant (K_b) was determined by plotting [DNA]/($\varepsilon_a - \varepsilon_f$) versus [DNA] according to the following equation:

$$\frac{[DNA]}{(\varepsilon_a - \varepsilon_f)} = \frac{[DNA]}{(\varepsilon_b - \varepsilon_f)} + \frac{1}{[K_b(\varepsilon_b - \varepsilon_f)]} \quad (6)$$

where [DNA] is the molar concentration of DNA in base pairs, ε_a, ε_f and ε_b are the apparent, free and fully bound complex extinction coefficients, respectively. Particularly, ε_f was evaluated from the calibration curve of the isolated metal complex, verifying Beer"s law. ε_a was evaluated as the ratio between the determined absorbance and the M(II) complex concentration, A_{obs}/[complex]. The data conformed to the above equation with a slope equal to $1/(\varepsilon_b - \varepsilon_f)$ and *y*-intercept equal to $1/K_b(\varepsilon_b - \varepsilon_f)$ and K_b was obtained from the ratio of slope to intercept. The standard Gibb"s free energy for DNA binding was evaluated from the following relation:[11,12,18,21]

$$\Delta G_b^* = -RT \ln K_b \quad (7)$$

2.9.3 | Hydrodynamic measurements for DNA interaction

Viscosity measurements were executed using an Oswald micro-viscometer, maintained at constant temperature of 25 °C. The fluidity times were recorded for various concentrations of the complexes (5–50 μM), maintaining the concentration of CT-DNA constant (260 μM). Mixing of the solution was achieved by bubbling nitrogen gas through the viscometer. The mean value of three measures was used to determine the viscosity of the samples. The buffer fluidity time in seconds was registered as $t°$. The relative viscosities for DNA in the presence (η) and absence ($\eta°$) of the complexes were evaluated using the relation $\eta = (t - t°)/t°$, where t is the observed fluidity time in seconds and the relative viscosity ($\eta/\eta°$) was determined against $1/R$ (R = [DNA]/[complex]).[18,19,21]

2.9.4 | Agarose gel electrophoresis measurements

The DNA binding studies were conducted using the agarose gel electrophoresis method.[19] Stock solutions of complexes were prepared by dissolving 20 mg of the prepared complexes in 20 ml of DMF. The sample (25 μg ml^{-1}) was added to CT-DNA and incubated for 1 h at 37 ± 1 °C. Then 30 μl of DNA sample (mixed with bromophenol blue dye at a 1:1 ratio) was transferred to the electrophoresis chamber wells along with a standard DNA marker in TBE buffer (50 mM Tris base, pH = 7.2; 1 mM EDTA/1 L) and then loaded onto the agarose gel. Then a constant vloyage (60 V) was used for about 45 min. Finally, the gel was removed and stained with 20 μg ml^{-1} ethidium bromide for 10–20 min. The bands acquired was spotted under UV light using a transilluminator followed by photography with a DMC-LZ5 Lumix digital camera to determine the extent of DNA binding compared with the standard DNA marker.[18–21]

2.10 | Anticancer activity

The anticancer activity was evaluated at the National Cancer Institute, Cancer Biology Department, Pharmacology Department, Cairo University. The absorbance or optical density (OD) of each well was measured spectrophotometrically at 564 nm with an ELISA microplate reader (Σ960, Meter Tech, USA). Evaluation of the cytotoxic activity of the prepared pro-ligand and its complexes was carried out against human colon carcinoma cells (HCT-116 cell line), hepatic cellular carcinoma cells (HepG-2 cell line) and breast carcinoma cells (MCF-7 cell line). The evaluation process was carried out *in vitro* using sulforhodamine B stain.[12,23–25] Cells were placed in a 96-multiwell plate (10^4 cells per well) for 24 h before adding the complexes to allow attachment of

cells to the walls of the plate. Various concentrations of the compounds under test in DMSO (0, 1, 2.5, 5 and 10 μM) were added to the cell monolayer. Monolayer cells were incubated with the complexes for 48 h at 37 °C and in an atmosphere of 5% CO_2. After 48 h, cells were fixed, rinsed and stained with sulforhodamine B stain.[12,23] Excess stain was washed with acetic acid and attached stain was treated with Tris–EDTA buffer. Colour intensity was measured in an ELISA reader. IC_{50} was evaluated and potency was calculated with regard to percentage change of vistabline standard.[12,23] The inhibitory concentration percent (IC %) was estimated[12,23–25] according to the equation:

$$\text{IC}\ (\%) = \frac{(\text{Control OD}) - (\text{ligand OD})}{\text{Control OD}} \times 100 \qquad (8)$$

3 | RESULTS AND DISCUSSION

3.1 | Physicochemical properties of HNAP imine pro-ligand and its complexes

3.1.1 | ^{1}H NMR and ^{13}C NMR spectra of HNAP imine pro-ligand

The formation of the prepared HNAP imine pro-ligand was further supported by the NMR spectral study. The ^{1}H NMR and ^{13}C NMR spectral data of the prepared pro-ligand are recorded in Section 1 (Figures S1 and S2). The ^{1}H NMR spectrum of HNAP imine pro-ligand shows two singlet signals at 15.65 and 9.50 ppm that are assigned to the two phenolic ─OH. Also, it shows a singlet signal at 9.49 ppm which is characteristic for azomethine (CH═N) proton of the pro-ligand.[26] Moreover, it shows multiplet signals at 8.36–6.83 ppm for aromatic CH (9) protons. Furthermore, it shows one proton doublet at position 10. The ^{13}C NMR spectrum of HNAP imine pro-ligand exhibits a signal at 177.17 ppm which may be assigned to azomethine carbon. The signals observed in the region 150.46–108.35 ppm are assigned to phenyl carbons.

3.1.2 | Elemental analysis and electrical conductivity measurements

All the prepared complexes are coloured, solid, stable at room temperature and non-hygroscopic in nature.

The elemental analysis results for the imine pro-ligand and its complexes are recorded in Table 1 and suggest that HNAP imine pro-ligand acts as a tridentate ligand and forms complexes with VO(II), Cr(III) and Ni(II) in metal-to-ligand ratio of 1:1 (Scheme 1). The molar conductance of all the prepared complexes was measured at room temperature in DMF as a solvent and the results are recorded in Table 1. The molar conductance values of all prepared complexes at room temperature fall in the range 2.1–9.4 Ω^{-1} cm^2 mol^{-1} indicating their non- electrolytic nature.[11,12,18–22,27]

3.1.3 | IR spectra

The bonding of the prepared HNAP imine pro-ligand to the metal ions was judged by a careful comparison of the IR spectra of the metal complexes with that of the free ligand. The characteristic IR frequencies of the HNAP pro-ligand and its complexes along with their assignments are summarized in Table 2. Bands due to ─OH and ─CH═N are distinguishable and offer proof regarding the structure of the pro-ligand and its bonding with metals. A band at 1632 cm^{-1} in the HNAP pro-ligand spectrum is due to ─C═N stretching vibration. On complexation, this band is displaced to a lower frequency (1597–1623 cm^{-1}). The negative shift of this band is an obvious indication of the involvement of the azomethine nitrogen atoms in complex formation.[10,26] This is supported by the appearance of bands at 561–670 cm^{-1} corresponding to the stretching vibration of M─N bond. Bands at 460–573 cm^{-1} correspond to M─O stretching vibrations. Band at 3448 cm^{-1} observed in the pro-ligand spectrum is due to stretching vibrations of free

TABLE 1 Analytical and physical data of HNAP imine pro-ligand and its complexes

Compound (molecular formula)	Molecular weight	Colour (yield, %)	Λ_m (Ω^{-1} cm^2 Mol^{-1})	μ_{eff} (BM)	M.p. And Dec. temp. (°C)	Analysis (%) Found (calcd)		
						C	H	N
HNAP ($C_{17}H_{13}NO_2$)	263.09	Yellow (88)	-	-	140	77.41 (77.52)	4.91 (4.98)	5.28 (5.32)
HNAPCr ($C_{17}H_{19}N_2CrO_9$)	447.00	Orange (86)	9.40	3.70	(220)	45.53 (45.64)	4.28 (4.25)	6.31 (6.26)
HNAPNi ($C_{17}H_{14}NNiO_{3.5}$)	346.70	Bright green (87)	6.30	2.65	(280)	58.79 (58.84)	4.07 (4.04)	4.10 (4.04)
HNAPV ($C_{17}H_{13}NO_4V$)	345.94	Brown (89)	2.10	1.78	(180)	58.85 (58.97)	3.80 (3.76)	4.01 (4.05)

TABLE 2 Characteristic IR bands (cm^{-1}) of HNAP imine pro-ligand and its complexes

Compound	υ(oh)/H_2O	$\upsilon(CH)_{ar}$	υ(C=N)	$\upsilon(C{-}O)_{ph}$	Bands due to (NO_3)			ν(M—N)	ν(M—O)
					$\upsilon(NO_2)_{as}$	$\upsilon(NO_2)_{sy}$	υ(no)		
HNAP	3448 (s)	3120	1632	**1240**	—	—	—	—	—
HNAPCr	3529	3321	1623	**1212**	1470	1356	858	567	460
HNAPNi	3422	3060	1620	1211	—	—	—	561	506
HNAPV	3423	3053	1597	1206	—	—	—	670	573

vs = very strong, s = strong, m = medium, b = broad, w = weak, ar = aromatic, py = pyridine, ph = phenolic, asy = asymmetric, sy = symmetric.

—OH. For the complexes, the recorded IR spectra show broad bands at 3422–3529 cm^{-1} which correspond to ν(OH) stretching vibration of crystalized water molecules, in accordance with the findings of the elemental analysis listed in Table 1. A band at 968–976 cm^{-1} (OH rocking) suggests the presence of coordinated water in all three complexes. In the low-frequency region, the HNAP imine pro-ligand shows an absorption band at 1240 cm^{-1} which can result from the stretching vibration of the phenolic (C—O) group. The shifting of that band to lower wavenumber on coordination shows that the oxygen atoms of the phenolic groups are coordinated to the metal ion. The characteristic frequencies of the coordinated nitrate group in HNAPCr complex possess three non-degenerate modes at 1470 cm^{-1} $\nu(NO_2)_{asy}$, 1356 cm^{-1} $\nu(NO_2)_{sy}$ and 858 cm^{-1} ν(NO).[28]

3.1.4 | Electronic spectra

Molecular electronic absorption spectra are often very significant in the evaluation of results furnished by other methods of investigation. The values of the maximum absorption wavelength (λ_{max}) and the molar absorptivity (ε_{max}) are listed in Table S1 and the spectra are presented in Figure 1. The electronic spectral measurements were used for assigning

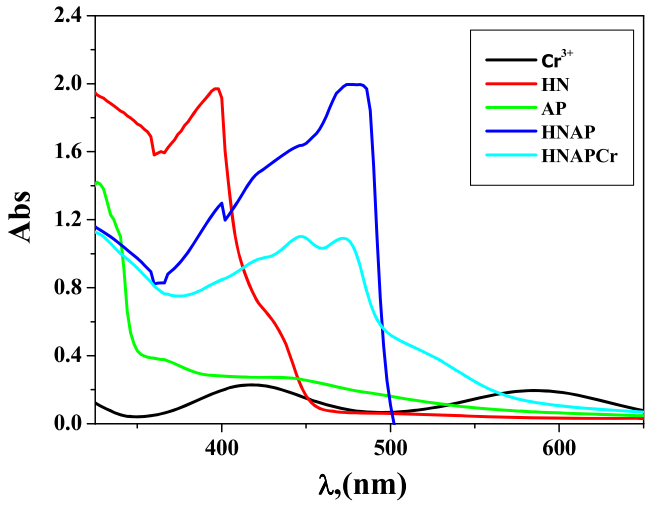

FIGURE 1 Molecular electronic spectra of HNAPCr complex and its components in DMF at 298 K

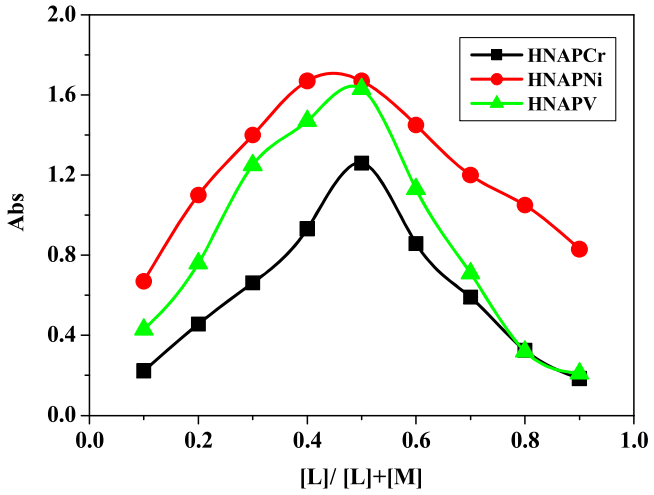

FIGURE 2 Job"s plots for determining the stoichiometry of the prepared complexes in aqueous ethanolic medium at [HNAPCr] = [HNAPNi] = [HNAPV] = 10^{-3} M and 298 K

the stereochemistry of metal ions in the complexes relying on the sites and number of d–d transition peaks.[29] The electronic absorption spectra of pro-ligand and its complexes were recorded in the wavelength range 200–800 nm and 298 K. The pro-ligand presents absorption bands in the UV–visible region around 400 nm which is assigned to n → π* transition originating from the imine function of the pro-ligand.[30] The absorption bands of complexes at λ_{max} = 318–472 nm are assigned to charge transfer within HNAP imine pro-ligand to the metal ion. Furthermore, there is a long and a broad band lying in the region 504–524 nm (ε_{max}= 230–570 mol^{-1} cm^2). This band could mainly correspond to the d → d transition in the structure of the complexes (Table S1).[31]

3.1.5 | Magnetic moment measurements

Magnetic susceptibility measurements offer information concerning the geometric structure of the compounds. The observed magnetic moments for complexes are generally diagnostic of the coordination geometry about the metal ion (Table1). HNAPCr complex shows magnetic moment corresponding to three unpaired electrons, i.e. 3.7 BM, as expected

for octahedral Cr(III) complexes.[32] The magnetic moment values of the Ni(II) complex is 2.65 BM, indicating the presence of two unpaired electrons per Ni(II) ion and suggesting this complex to have tetrahedral geometry.[33] The HNAPV complex has a magnetic moment value of 1.78 BM, which is close to the spin-only value for d^1 and in agreement with the reported values for square pyramidal and distorted octahedral complexes of VO(II).[34]

3.1.6 | Thermal analysis

Thermal analysis of metal chelates is an important tool for (i) obtaining information about the thermal stability of these complexes and (ii) indicating if the water molecules (if present) are inside or outside the interior coordination sphere of the central metal ion. The thermograms of the prepared imine complexes indicate the presence of one molecule of coordinated water in the case of HNAPV and HNAPNi complexes and two coordinated water molecules in the case HNAPCr complex (Scheme 1).[33] The thermal behaviour of the metal complexes shows dehydration of water molecules in the first step; then loss of coordinated water molecules with degradation of the pro-ligand molecule in the next steps as shown in Table 3. The thermogram of the HNAPCr complex shows five degradation steps within the temperature range 35–567 °C. The first stage at 35–110 °C corresponds to the elimination of two water molecules of hydration, with a mass loss of 8.12% (calcd 8.05%). The second step at 112–211 °C corresponds to the removal of two coordinated water molecules with mass loss of 8.22% (calcd 8.05%). The third step at 213–285 °C corresponds to the loss of nitrate group (NO_3)with a net weight loss of 13.78% (calcd 13.77%). Also, the HNAPCr complex shows mass loss within the temperature ranges 287–399 and 401–567 °C, which are due to removal of part of the pro-ligand ($C_{10}H_6O$) and (C_7H_5NO) with mass losses of 31.65% (calcd 31.77%) and 26. 52% (calcd 26.6%), respectively. Finally metallic residue is the final product of thermal decomposition with mass loss of 11.70% (calcd 11.63%).[35] The thermal analysis curve of the HNAPNi complex shows four stages of decomposition within the temperature range 40–595 °C. The first stage at 40–115 °C corresponds to the elimination of half a water molecule of hydration, with a mass loss of 2.75% (calcd 2.6%). The second step at 116–222 °C corresponds to the removal of one coordinated water molecules with mass loss of 5.00% (calcd 5.19%). The third stage of decomposition occurs in the temperature range 223–381 °C with a net weight loss of 34.37% (calcd 34.32%) which is consistent with the removal of part of the pro-ligand (C_7H_5NO) molecule. The fourth step involves the loss of the other part of the pro-ligand to give finally Ni as a residue. The final product explained from a horizontal curve being obtained suggesting formation of metal product.[36] HNAPV complex exhibits no mass loss up to 137 °C, indicating the absence of hydrated water molecules. The first step of decomposition within the temperature range 137–180 °C corresponds to the loss of one coordinated water molecule, with a mass loss of 5.07% (calcd 5.20%).[37] The third and fourth steps within the temperature range 182–552 °C involve removal of organic ligand moiety to give finally VO residue with a net weight loss of 19.33% (calcd 19.35%).

TABLE 3 Thermal degradation steps, mass losses, proposed lost segments, final residue and thermo-kinetic activation parameters of each decomposition step for the prepared complexes

Complex	Dec.temp. (°C)	Mass loss (%) Found	(calcd)	Proposedsegment	E^*(kJ Mol^{-1})	A(s^{-1})	ΔH^* (kJ Mol^{-1})	ΔG^* (kJ Mol^{-1})	ΔS^* (J Mol^{-1} K^{-1})
HNAPCr	35–110	8.12	(8.05)	$2H_2O$	78.30	0.096	77.8	93.6	−251.55
	110–211	8.22	(8.05)	$2H_2O$			78.3	119.7	−259.52
	211–285	13.78	(13.87)	NO_3			76.0	141.7	−262.97
	285–399	31.65	(31.77)	$C_{10}H_6O$			75.5	165.8	−265.50
	399–567	26.52	(26.60)	C_7H_5NO			74.2	205.8	−268.57
Residue	>567	11.70	(11.63)	Cr			—	—	—
HNAPNi	40–115	2.75	(2.60)	$0.5H_2O$	32.8	0.049	32.2	49.5	−257.62
	116–222	5.00	(5.19)	H_2O			31.4	76.0	−265.30
	223–381	34.37	(34.32)	C_7H_5NO			30.3	111.9	−270.14
	384–595	41.05	(40.95)	$C_{10}H_6O$			28.7	163.9	−274.21
Residue	>595	16.83	(16.93)	Ni			—	—	—
HNAPV	137–180	5.07	(5.20)	H_2O	135.2	0.40	134.0	174.0	−247.40
	182–326	34.49	(34.40)	C_7H_5NO			133.0	196.0	−251.14
	328–552	41.13	(41.05)	$C_{10}H_6O$			131.5	246.0	−255.90
Residue	>552	19.33	(19.35)	VO			—	—	—

3.1.7 | Kinetic aspects

The kinetic parameters are given in Table 3. It is evident that G^* values increase with increasing temperature. The positive values of H^* indicate that degradation processes are endothermic. In most thermal steps, S^* values are negative suggesting a degradation via an abnormal pathway for those steps and the degradation processes are undesirable. The negative activation entropy values give evidence for a more ordered activated state. This can occur through the chemisorption of oxygen and other decomposition products. The more ordered nature can be referred to the bond polarization of the activated state which takes place through electronic transitions. Finally, positive values of H^* and G^* represent the endothermic character for all thermal steps.[38]

3.1.8 | Spectrophotometric determination of stoichiometry of complexes

Stoichiometry of the prepared complexes was determined using two methods including the use of spectrophotometry, namely continuous variations method and molar ratio method. Based on the obtained results, the stoichiometry of the prepared complexes is 1:1. The curves of the continuous variation method (Figure 2).display maximum absorbance at mole fraction $X_{\text{ligand}} = 0.5–0.6$ showing the complexation of metal ions to ligand in a molar ratio of 1:1. Moreover, the data from the molar ratio method support the same metal ion to ligand ratio of the prepared complexes (Fig. S3).[11,12,18,22]

3.1.9 | Determination of apparent formation constants of complexes

The formation constants (K_f) of the studied imine complexes formed in solution were obtained from spectrophotometric measurements by utilizing the continuous variation method (Table S2), where A_m is the absorption at the maximum of the complex, A is arbitrarily selected absorbance values on either side of the absorbance peak and C is the elementary concentration of the metal. The obtained K_f values show the high stability of the complexes. The values of K_f for the complexes decrease in the following order: HNAPCr > HNAPV > HNAPNi. Moreover, the stability constant (pK) and Gibbs free energy ($\Delta G^{\neq}$) values of the complexes were calculated. The negative values of Gibbs free energy show that the reaction is spontaneous and favoured. The pH profilse (absorbance versus pH) depicted in Figure 3 show typical dissociation curves and a high stability range of pH (4–9) of tested complexes. This shows that the formation of the complexes greatly stabilizes the prepared imine pro-ligand. Consequently, the desired pH range for different applications of the tested complexes is from pH = 4 to 9. Based on the obtained results of elemental analyses, molar conductance, magnetic measurements, IR and electronic spectra, the suggested composition of the complexes was identified.

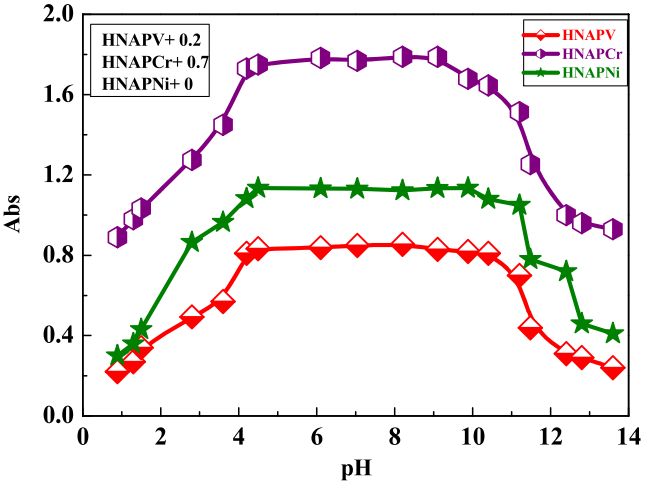

FIGURE 3 Dissociation curves of prepared imine complexes in DMF

3.2 | Antimicrobial activity evaluation

The *in vitro* antimicrobial activities of the HNAP imine pro-ligand and its complexes against three selected bacteria and three fungi were determined. Any chemotherapeutic agent inhibits the growth of microbes by microstatic mechanisms. All of the compounds display good biological activity against the microorganisms. On contrasting the biological activity of the imine pro-ligand and its complexes with those of standard bactericide and fungicide, it is clear that the complexes have moderate activity as compared with the standard, but all the complexes are more active than free pro-ligand. The greater inhibition zone of the transition metal complexes than those of the pro-ligand can be considered based on the Overtone notion and chelation theory. Upon chelation, the polarity of the metal ion is decreased to a great extent due to the overlap of the ligand orbital and the fraction of the positive charge of the metal ion participating with donor groups. Furthermore, it increases the delocalization of the π-electrons over the whole chelating ring and increases the breakthrough of the complexes into lipid membranes and the blocking of the metal attachment locations in the enzymes of microorganisms.[12,23,39] The conclusions of the investigations account for the antipathogenic manner of the compounds and this efficacy is positively changed on complexation. Data are listed in Table 4 and shown in Figures 4 and 5. The minimum inhibitory concentration (MIC) was estimated by the serial dilution route and is reported in Table 5. The HNAPV complex (3 mg ml^{-1}) is found to be highly effective as its exhibits the lowest MIC against *Bacillus subtilis* bacterium and *A. flavus* fungus compared to the other compounds. The

TABLE 4 Results of antibacterial and antifungal bioassay of HNAP imine pro-ligand and its complexes against different strains of bacteria and fungi

Compound	± SD inhibition zone (mm)											
	Escherichia coli (−ve)		*Bacillus subtilis* (+ve)		*Staphylococcus aureus* (+ve)		*Candida albicans*		*Aspergillus flavus*		*Trichophyton rubrum*	
Conc. (mg ml^{-1})	10	20	10	20	10	20	10	20	10	20	10	20
HNAP	4 ± 0.23	10 ± 0.05	5 ± 0.17	13 ± 0.27	4 ± 0.63	12 ± 0.88	4 ± 0.05	7 ± 0.55	3 ± 0.11	6 ± 0.82	2 ± 0.10	5 ± 0.04
HNAPV	13 ± 0.29	28 ± 0.11	16 ± 0.19	37 ± 0.87	13 ± 0.33	31 ± 0.41	17 ± 0.25	27 ± 0.41	10 ± 0.29	22 ± 0.19	9 ± 0.12	17 ± 0.80
HNAPNi	12 ± 0.53	26 ± 0.66	13 ± 0.09	32 ± 0.13	12 ± 0.07	29 ± 0.39	11 ± 0.22	17 ± 0.10	7 ± 0.22	15 ± 0.14	6 ± 0.10	11 ± 0.19
HNAPCr	14 ± 0.22	30 ± 0.76	17 ± 0.91	39 ± 0.32	14 ± 0.61	32 ± 0.08	14 ± 0.33	24 ± 0.14	9 ± 0.55	20 ± 0.9	8 ± 0.10	15 ± 0.59
Gentamycin	20 ± 0.71	40 ± 0.33	26 ± 0.15	51 ± 0.72	25 ± 0.93	45 ± 0.11	—	—	—	—	—	—
Fluconazol	—	—	—	—	—	—	24 ± 0.55	37 ± 0.62	16 ± 0.49	31 ± 0.88	15 ± 0.71	25 ± 0.90

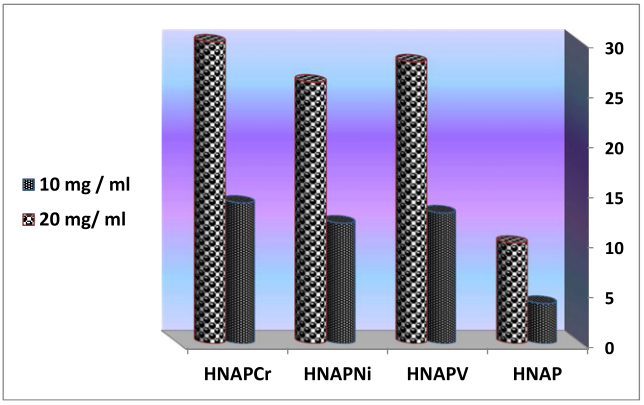

FIGURE 4 Histogram showing the comparative antibacterial activities of prepared compounds (HNAP, HNAPCr, HNAPNi and HNAPV) against *E. coli* bacteria

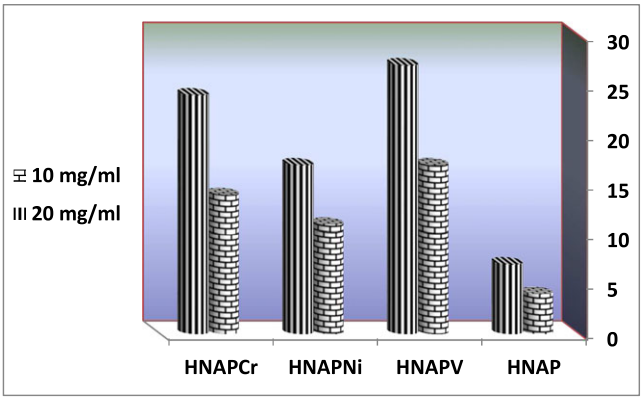

FIGURE 5 Histogram showing the comparative antifungal activities of prepared compounds (HNAP, HNAPCr, HNAPNi and HNAPV) against *C. albicans* fungus

antimicrobial studies suggest that all the complexes exhibit promoted antimicrobial activity against microbial strains in comparison to the free pro-ligand. Previous studies suggested that chelation tended to make the pro-ligand a more powerful and potent bacteriostatic agent,[40] thus inhibiting the growth of microbes more than the pro-ligand, which is similar to the results of this study. It is suspected that factors such as solubility, conductivity, dipole moment and cell permeability influenced by the existence of metal ion might be a possible reason for the increase in activity. The activities of the prepared complexes were confirmed by calculating the potency index (Table S3) according to the following relation:[11,12,22]

$$\text{Activity index } (A) = \frac{\text{Inhibition zone of complex (mm)}}{\text{Inhibition zone of standard drug (mm)}} \times 100 \quad (9)$$

The variation in the activity of the metal complexes against different microbes depends either on the difference in the ribosomes of the microbial cells or on the impermeability of the cells of the microbes. The lower activity of complexes as

TABLE 5 Minimum inhibition concentration (MIC) for antimicrobial assay of the ligand and its complexes

	Bacteria			Fungi		
Compound	***S. aureus***	***E. coli***	***B. subtilis***	***A. flavus***	***C. albicans***	***T. rubrum***
HNAP	7.0	8.0	7.5	6.0	6.5	7.0
HNAPV	4.5	3.5	3.0	3.0	4.0	3.5
HNAPNi	6.0	5.5	6.0	3.5	5.0	4.0
HNAPCr	5.0	4.5	5.5	3.5	5.0	4.5

compared to others may be attributed to low lipid solubility, so that the metal ion may not be able to reach the favourable site of action of the cell wall to interfere with normal cell activity. Although chelation itself plays a significant role in determining antibacterial behaviour of the complexes, concurrently various factors such as solubility, size, dipole moment, coordinating sites, redox potential of metal ion, solubility, bond length between metal and ligand, geometry of complexes, steric factors, pharmacokinetics, concentration and hydrophobicity have substantial influence on the antibacterial activity. Thus, it is apparent from the results that enhanced antibacterial activity of the metal complexes may be due not only to chelation but also intricate combinations of several other factors as well.[40]

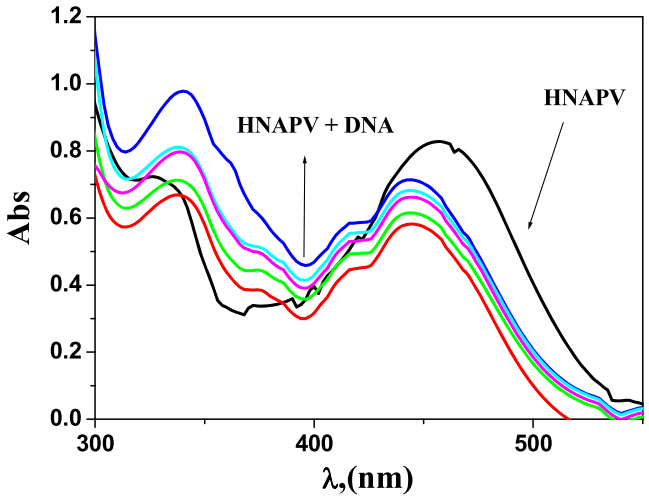

FIGURE 6 Spectral scans of interaction of HNAPCr complex (10^{-3} M) in 0.01 M tris buffer (pH = 7.2, 298 K) with CT-DNA (0–30 μM, from top to bottom)

3.3 | DNA binding potency

3.3.1 | Electronic spectra of interaction with DNA

Titration with electronic absorption spectroscopy is an attractive route to investigate the binding mode of DNA with metal complexes. The spectra were recorded as a function of the addition of buffer solutions of pure CT-DNA to buffer solutions of the tested complexes. If the interaction mode is intercalation, the orbital of the inserted ligand can couple with the orbital of the base pairs, lowering the π–π* transition energy and leading to bathochromism. If the conjunction orbital is partially filled by electrons, it results in reduction of the transition probabilities and leads to hypochromism.[12,22] The extent of hypochromism or hyperchromism in the metal-to-ligand charge transfer band is commonly consistent with the force of intercalation interaction.[11,23] The electronic absorption spectra of HNAPCr complex in the absence and presence of various concentrations of buffered CT-DNA are shown in Figures 6 and S4. Addition of increasing amounts of CT-DNA results in a reduction of absorbance for a complex. The spectral parameters and K_b for DNA interaction with the tested complexes are summarized in Table 6. The investigated complexes can bind to DNA mainly via

TABLE 6 Spectral parameters for interaction of imine complexes

Complex	λ_{max}, free (nm)	λ_{max}, bound (nm)	Δn	Chromism (%)[a]	Type of chromism	Binding constant, K_b ($\times 10^4$ mol^{-1} dm^3)	ΔG^* (kJ Mol^{-1})
HNAPCr	442	444	2	26.20	Hyper	11.51	−28.87
	464	466	2	15.84	Hyper		
	348	356	8	164.18	Hyper		
HNAPNi	447	441	6	28.70	Hypo	1.69	−24.12
	470	463	7	24.43	Hypo		
	236	237	1	33.00	Hypo		
HNAPV	458	444	14	14.46	Hyper	7.68	−27.87
	327	338	11	34.67	Hyper		

[a]Chromism (%) = $(Abs_{free} - Abs_{bound})/Abs_{free}$.[11,12,18,22]

intercalative and replacement modes with the sequence: HNAPCr > HNAPV > HNAPNi (Scheme 2a).

3.3.2 | Viscosity measurements

For explaining the nature of interaction between the tested complexes and DNA, viscosity measurements were carried out. Hydrodynamic methods such as viscosity measurements which are sensitive to length increase or decrease of DNA are regarded as the most effective routes of studying the binding mode of compounds to DNA in the absence of crystallographic structural data and NMR data. For further explaining the binding mode, viscosity measurements were made. Under appropriate conditions, a traditional intercalative mode such as intercalation of drugs like ethidium bromide leads to a significant increase in the viscosity of DNA solution due to an increase in the segregation of base pairs at the intercalation site and hence an increase in the overall DNA length. On the other hand, drug molecules attaching exclusively to the DNA grooves lead to less pronounced DNA solution viscosity.[22,41] A partial intercalation of a compound may bend the DNA helix, resulting in the reduction of its effective length and, concomitantly, its viscosity.[12,22,42–44] The relative viscosity of DNA solution increases significantly as the amount of compound increases, as shown in Figure 7. This may be due to the admission of the aromatic ring in the imine pro-ligand into the DNA base pairs resulting in a distortion in the DNA helix, and hence an increase in the segregation of the base pairs at the intercalation place and an increase in DNA molecular length. Moreover, the sequence of the observed increase in the values of viscosity is related with the binding affinity to DNA, i.e. HNAPCr complex shows the highest binding affinity to DNA and the highest

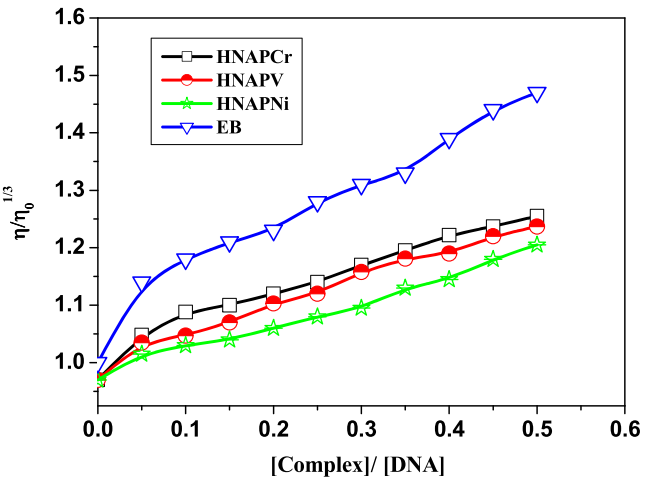

FIGURE 7 Effect of increasing concentration of prepared complexes on relative viscosities of DNA at [DNA] = 0.5 mM, [complex] and [ethidium bromide] = 25–250 μM and 298 K

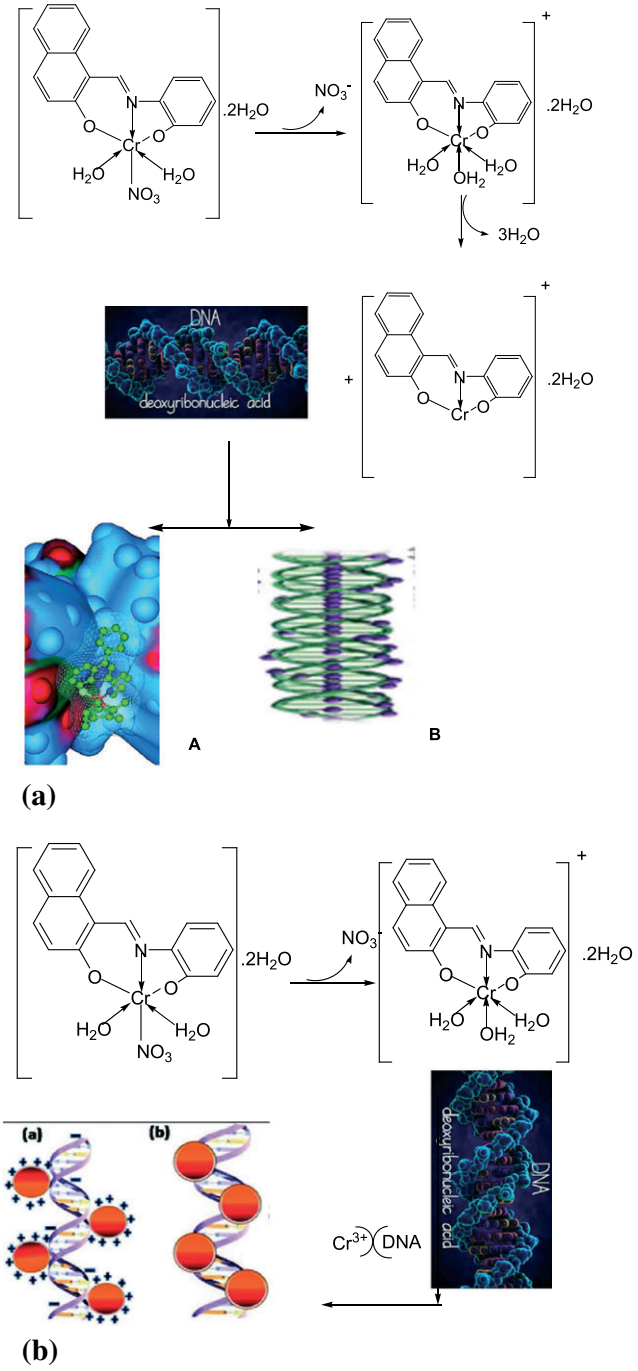

SCHEME 2 **(a)** suggested mechanism for interaction of HNAPCr complex with DNA via (a) intercalation binding and (B) replacement. **(b)** suggested mechanism for interaction of HNAPCr complex with DNA via electrostatic binding

viscosity. Moreover, HNAPCr complex could bind to DNA via electrostatic binding as shown in Scheme 2(b). Electrostatic binding may occur due to water molecules replacing coordinated nitrate group. Thus, HNAPCr complex will be charged (Scheme 2b) and electrostatic interaction occurs between the positive charge in the complex and base pairs of DNA.

3.3.3 | Gel electrophoresis

Agarose gel electrophoresis was used for the DNA binding studies. The prepared imine chelates were studied for their DNA binding activity using the agarose gel electrophoresis method (Figure 8). The gel after electrophoresis clearly showed that the intensity of all the treated DNA samples has partially decreased, possibly because of the interaction with DNA. The partial binding of DNA was observed for the prepared imine chelates. The difference is clarified in the bands of the complexes compared to that of the control DNA. The control DNA alone does not show any visible cleavage whereas the complexes show cleavage.[22,44] However, the nature of reactive intermediates involved in the DNA binding by the complexes is not obvious.[45] These results show that the metal ions play an important role in the interaction with isolated DNA. As the compounds are observed to bind with DNA, it can be concluded that the compounds reduce the growth of the pathogenic organisms by interaction with the genome. The studies reveal that there is partial binding of DNA with VO(II), Cr(III) and Ni(II) imine complexes. The experimental results suggest that the complexes could bind to DNA via intercalative mode.

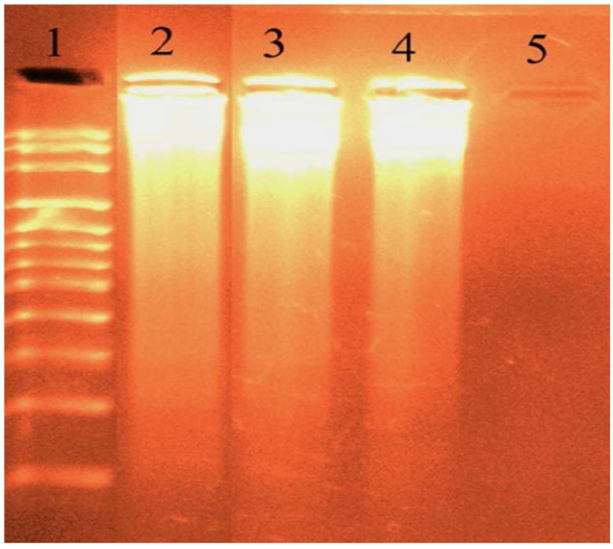

FIGURE 8 DNA binding results of prepared imine complexes based on gel electrophoresis. Lane 1: DNA ladder; lane 2: HNAPV + DNA; lane 3: HNAPCr + DNA; lane 4: HNAPNi + DNA; lane5: HNAPV complex

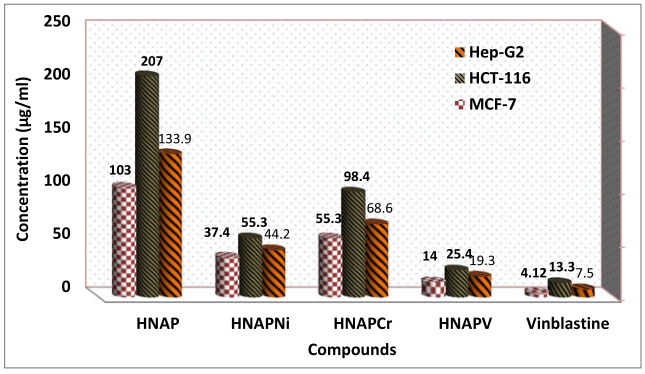

FIGURE 9 IC_{50} values of HNAP imine pro-ligand and its complexes against HCT-116, HepG-2 and MCF-7 cell lines

3.4 | Anticancer activity

The cytotoxic potency of the prepared HNAP imine pro-ligand and its complexes was evaluated against HCT-116 HepG-2 and MCF-7 cell lines within the concentration range 0–10 µM. The IC_{50} values were evaluated for each compound and the results are shown in Figure 9 and Table S4. As shown, most complexes display manifestly cytotoxic potencies (which are greater than that of the ligand) compared to vinblastine standard drug. It seems that changing the complexation locations and the nature of the metal ion has an impact on the biological activity. Cytotoxicity of the complexes may be due to the focal metal atom which was considered in Tweedy"s chelation theory.[46,47] Cytotoxicity conclusions indicated that all tested complexes (IC50 = 25.4 – 98.4 µg/µl) demonstrated potent cytotoxicity against HCT-116 cancer cells, (IC50 = 19.3 – 68.6 µg/µl) demonstrated potent cytotoxicity against HepG-2 cancer cells and (IC50 = 14 – 55.3 µg/µl) against MCF-7 cancer cells. HNAP V complex shows the highest cytotoxicity effect with IC_{50} value of 14 µg $µl^{-1}$, followed by HNAPNi complex with IC_{50} value of 37.4 µg $µl^{-1}$ and then HNAPCr complex with IC_{50} value of 55.3 µg $µl^{-1}$ in the case of all tested cancer cells. It is observed also that all complexes are more potent than the free pro-ligand. This indicates the benefits of the anti-tumour potency upon coordination. The cytotoxic potency may be explained in that the positive charge of the metal increases the acidity of coordinated pro-ligand that gives protons, causing more potent hydrogen bonds which enhance the biological activity.[22,47] It seems that changing the coordination locations and the nature of the metal ion has a clear effect on the biological activity by modifying the binding ability to DNA.[12,48] Gaetke and Chow reported that metal has been suggested to smooth oxidative tissue damage through a free-radical mediated trajectory analogous to the Fenton reaction.[49]

4 | CONCLUSIONS

In this study, three innovative VO(II), Cr(III) and Ni(II) imine complexes have been synthesized and their structures have been characterized using physicochemical and spectral tools. The obtained results demonstrated that the HNAP imine pro-ligand behaves as a dibasic tridentate ONO ligand and coordinates to VO(II), Cr(III) and Ni(II) in a 1:1 molar ratio. From the analytical and spectral data, it is observed that the complexes adopted octahedral geometry in the case of Cr(III), tetrahedral geometry in the case Ni(II) and distorted square pyramidal geometry in the case of VO(II). The antipathogenic screening showed that these complexes are good antimicrobial agents against various organisms as compared to standards. Moreover, the interaction of the complexes with CT-DNA has been effectively explored by electronic absorption, viscosity measurements and gel electrophoresis. The DNA interaction studies suggest intercalative and replacement modes of interaction. Furthermore, the growth inhibitory effect of the prepared compounds was tested on HepG-2, HCT-116 and MCF-7 cancer cells. Among these compounds, HNAPV significantly decreases cell viability in time- and dose-dependent manners. These biological findings from our study would be helpful in exploring the interaction of DNA exposed to metal complexes and may lead to progress in improvement of novel metal-based therapeutic drugs.

REFERENCES

[1] L. H. Abdel-Rahman, R. M. El-Khatib, L. A. E. Nassr, A. M. Abu-Dief, *Int. J. Chem. Kin.* **2014**, *46*, 543.

[2] A. M. Abu-Dief, M. S. M. Abdelbaky, S. García-Granda, *Acta Crystallogr.* **2015**, *E71*, 496.

[3] L. H. Abdel-Rahman, R. M. El-Khatib, L. A. E. Nassr, A. M. Abu-Dief, *Russ. J. Gen. Chem.* **2014**, *84*, 1830.

[4] J. Tisato, F. Refosco, F. Bandoli, *Coord. Chem. Rev.* **1994**, *135*, 325.

[5] J. Lacroix, *Eur. J. Inorg. Chem.* **2001**, *2*, 339.

[6] A. M. Abu-Dief, R. Díaz-Torres, E. C. Sañudo, L. H. Abdel-Rahman, N. A. Alcalde, *Polyhedron* **2013**, *64*, 203.

[7] A. M. Abu-Dief, I. M. A. Mohamed, *J. Basic Appl. Sci.* **2015**, *4*, 119.

[8] C. Redshaw, *Dalton Trans.* **2010**, *39*, 5595.

[9] K. Nomura, S. Zhang, *Chem. Rev.* **2011**, *111*, 2342.

[10] L. H. Abdel-Rahman, R. M. El-Khatib, L. A. E. Nassr, A. M. Abu-Dief, M. Ismael, *J. Spectrochim. Acta A* **2014**, *117*, 366.

[11] L. H. Abdel-Rahman, A. M. Abu-Dief, S. K. Hamdan, A. A. Seleem, *Int. J. Nano Chem.* **2015**, *1*, 65.

[12] L. H. Abdel-Rahman, A. M. Abu-Dief, R. M. El-Khatib, S. M. Abdel-Fatah, *J. Photochem. Photobiol. B* **2016**, *162*, 298.

[13] A. Datta, N. K. Karan, S. Mitra, G. Rosair, *Z. Naturforsch.* **2002**, *576*, 999.

[14] D. Rehder, *Coord. Chem. Rev.* **1999**, *182*, 297.

[15] S. Y. Ebrahimipour, I. Sheikhshoaie, A. C. Kautzb, M. Ameri, H. Pasban-Aliabadi, H. A. Rudbari, G. Bruno, C. Janiak, *Polyhedron* **2015**, *93*, 99.

[16] S. Rayati, A. Ghaemi, N. Sadeghzadeh, *Catal. Commun.* **2010**, *11*, 792.

[17] H. Keypour, M. Rezaeivala, L. Valencia, P. Pérez-Lourido, *Polyhedron* **2008**, *27*, 3172.

[18] L. H. Abdel-Rahman, R. M. El-Khatib, L. A. E. Nassr, A. M. Abu-Dief, F. E. D. Lashin, *Spectrochim. Acta A* **2013**, *111*, 266.

[19] L. H. Abdel-Rahman, A. M. Abu-Dief, M. Ismael, M. A. A. Mohamed, N. A. Hashem, *J. Mol. Struct.* **2016**, *1103*, 232.

[20] A. M. Abu-Dief, L. A. E. Nassr, *J. Iran. Chem. Soc.* **2015**, *12*, 943.

[21] L. H. Abdel Rahman, A. M. Abu-Dief, N. A. Hashem, A. A. Seleem, *Int. J. Nano Chem.* **2015**, *1*, 79.

[22] L. H. Abdel-Rahman, A. M. Abu-Dief, E. F. Newair, S. K. Hamdan, *J. Photochem. Photobiol. B* **2016**, *160*, 18.

[23] A. M. Abu-Dief, I. F. Nassar, W. H. Elsayed, *Appl. Organometal. Chem.* **2016**, *30*, 917.

[24] S. S. Hindo, M. Frezza, D. Tomco, M. J. Heeg, L. Hryhorczuk, B. R. McGarvey, Q. P. Dou, C. N. Verani, *Eur. J. Med. Chem.* **2009**, *44*, 4353.

[25] M. I. Hossain, M. Switalska, W. Peng, M. Takashima, N. Wang, M. Kaiser, J. Wietrzyk, S. Dan, T. Yamori, T. Inokuchi, *Eur. J. Med. Chem.* **2013**, *69*, 294.

[26] L. H. Abdel-Rahman, A. M. Abu-Dief, M. S. S. Adam, S. K. Hamdan, *Catal. Lett.* **2016**, *146*, 1373.

[27] S. Chandra, S. Raizada, M. Tyagi, P. Sharma, *Spectrochim. Acta A* **2008**, *69*, 816.

[28] A. A. A. Emara, *Spectrochm Acta A* **2010**, *77*, 117.

[29] R. A. Kusanur, M. Ghate, M. V. Kulkarni, *J. Chem. Sci.* **2004**, *116*, 265.

[30] R. M. Silverstein, F. X. Webster, *Spectrometric Identification of Organic Compounds*, 6th ed., John Wiley, New York **1997**.

[31] L. H. Abdel-Rahman, A. M. Abu-Dief, R. M. El-Khatib, L. A. E. Nassr, *J. Mol. Struct.* **2013**, *1040*, 9.

[32] A. N. M. A. Alaghaz, M. E. Zayed, S. A. Alharbi, R. A. A. Ammar, *J. Mol. Struct.* **2015**, *1087*, 60.

[33] T. M. A. Ismail, A. A. Saleh, M. A. El Ghamry, *Spectrochim Acta A* **2012**, *86*, 276.

[34] S. Sarkar, K. Dey, S. Biswas, B. B. Bhaumik, *J. Coord. Chem.* **2007**, *60*, 1143.

[35] M. Montazerozohori, S. Mojahedi Jahromi, A. Masoudiasl, P. McArdle, *Spectrochim. Acta A* **2015**, *138*, 517.

[36] S. M. Pradeepa, H. S. B. Naik, B. V. Kumar, K. I. Priyadarsini, A. Barik, T. R. R. Naik, M. C. Prabhakara, *J. Spectrochim. Acta A* **2013**, *115*, 12.

[37] S. N. Azizi, S. E. Tilami, *Micropor. Mesopor. Mater.* **2013**, *167*, 89.

[38] T. A. Yousef, G. M. Abu El-Reash, I. M. Gabr, O. A. El-Gammal, R. A. Bedier, *J. Mol. Struct.* **2012**, *1029*, 149.

[39] Z. Khanam, C. S. Wen, I. Ul Haq Bhat, *J. King Saud Univ.* **2015**, *27*, 23.

[40] L. P. Nitha, R. Aswathy, N. E. Mathews, B. S. Kumara, K. Mohanan, *Spectrochim. Acta A* **2014**, *118*, 154.

[41] D. S. Raja, S. P. Bhuvanesh, K. Natarajan, *J. Biol. Inorg. Chem.* **2012**, *17*, 223.

[42] L. H. Abdel-Rahman, A. M. Abu-Dief, N. M. Ismail, *Inorg. Nano-Metal Chem.* **2017**, *47*, 467.

[43] Y. Liu, W. Mei, J. Lu, H. Zhao, L. He, F. Wu, *J. Coord. Chem.* **2008**, *61*, 3213.

[44] L. H. Abdel-Rahman, R. M. El-Khatib, A. M. Abu-Dief, S. M. Abdel-Fatah, A. A. Sleem, *Int. J. Nano Chem.* **2016**, *2*, 83.

[45] G. Yang, F. Z. Wu, L. Wang, L. Nian Fi, X. Tina, *J. Inorg. Biochem.* **1997**, *66*, 141.

[46] B. Tweedy, *Phytopathology* **1964**, *55*, 910.

[47] L. H. Abdel-Rahman, A. M. Abu-Dief, R. M. El-Khatib, S. M. Abdel-Fatah, *Bioorg. Chem.* **2016**, *69*, 140.

[48] G. Feng, J. C. Mareque-Rivas, N. H. Williams, *Chem. Commun.* *2006*, 1845.

[49] L. M. Gaetke, C. K. Chow, *Toxicology* **2003**, *189*, 147.

SUPPORTING INFORMATION

Additional Supporting Information may be found online in the supporting information tab for this article.

How to cite this article: Abdel-Rahman LH, Abu-Dief AM, Basha M, Hassan Abdel-Mawgoud AA. Three novel Ni(II), VO(II) and Cr(III) mononuclear complexes encompassing potentially tridentate imine ligand: Synthesis, structural characterization, DNA interaction, antimicrobial evaluation and anticancer activity. *Appl Organometal Chem*. 2017;e3750. https://doi.org/10.1002/aoc.3750